Wind Fabric Diagrams and Their Application to Wind Energy Analysis

BRIANT L. DAVIS AND MICHAEL W. EKERN

Institute of Atmospheric Sciences, South Dakota School of Mines and Technology, Rapid City 57701

(Manuscript received 14 September 1976)

ABSTRACT

By means of the Lambert projection, wind vector data may be plotted onto a frequency map. The resulting diagram portrays the "wind fabric" for the data sample of a single station or for groups of stations. The area-true distribution of wind vectors is thus given in great detail and allows several standard tests for homogeneity and anomaly significance. By using a "swinging plate" device the wind energy density and wind power can be calculated for any velocity-compass heading sector of the diagram desired and allows for a universal scaling of the velocity variable of the diagram.

1. Introduction

The position of a line or plane oriented in space can be described very conveniently on a stereographic projection by means of two angles. It is very commonly used in structural geology, petrofabrics and crystallography. The stereographic projection is simply the angular elements on the surface of a sphere projected onto the equatorial plane such that lines (or poles) produce a point on the projection and planes trace out great circles.

Of particular interest in both petrofabrics and in the development to follow is the Lambert equal area projection commonly known as the Schmidt net in petrofabrics (Fairbairn, 1949; Turner and Weiss, 1963). The particular value of the Lambert projection (or net) lies in the property that all zones of equal area on the surface of the reference sphere remain equal on the projection itself. This allows for contouring of point density on the projection as well as giving the appearance to the viewer that contours enclosing equal areas on both the center and periphery of the projection do in fact contain the same concentration of fabric elements. For details on the geometry of the stereographic and Lambert equal area projections the reader is referred to the Appendix.

2. Geometry and fabric characteristics

The frequency of wind velocity observations is generally expressed by the so-called rose diagram which consists of sectors of the compass extended in length to be proportional to the number of observations within that sector. The velocity of the wind within a sector can only crudely be demonstrated by the rose diagram; in general, it is accomplished by scaling portions within the sector indicating the percentage of observations falling within the discrete wind velocity categories. Even when the rose diagram is constructed from many sectors and "contoured" by connecting zones of equal frequency or velocity, very little accurate information is available with which to make statistical tests[1] and which can give the reader an area-true distribution (map) of the data.

Now in wind measurements the two variables are velocity and direction. The compass direction is already one of the variables easily plotted on the Lambert projection. The other variable, also an angle, must be either scaled to a velocity or by means of some physical analog calculated from some function of velocity or other measured parameter such as particulate concentration, pollen count, etc. When this scaling is accomplished, it is a simple matter to plot as points on a Lambert equal area projection every observation of wind direction and velocity (or pollution concentration, etc.). Using the standard contouring procedure used in petrofabrics, a probability map can then be constructed which gives the fine detail of variables: frequency, velocity and compass direction for the sample obtained. The reader is referred to the Appendix for details on point plotting and contouring procedures. The data can be plotted for one station or for several stations within a given area, for which the latter case presents an averaged picture of wind fabric over the region.

Figs. 1 and 2 present the point plot and contoured grid for 34 observations from seven Black Hills stations during June, July and August 1975. In this case, 90° of the vertical angular variable (measured from

[1] The chi-square test, *t*-test and Winchell zone test can be applied to the plotted data for analysis of homogeneity, anomaly significance, etc.

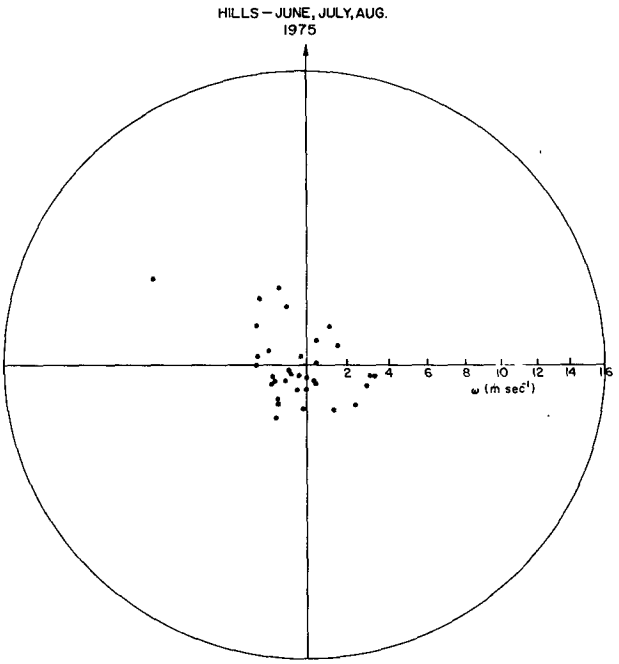

FIG. 1. Plot of 34 wind vectors from Black Hills stations of western South Dakota on the Lambert projection. Horizontal angle is compass heading; vertical angle (from center) is scaled so that $\pi/2 = 16.1$ m s^{-1}.

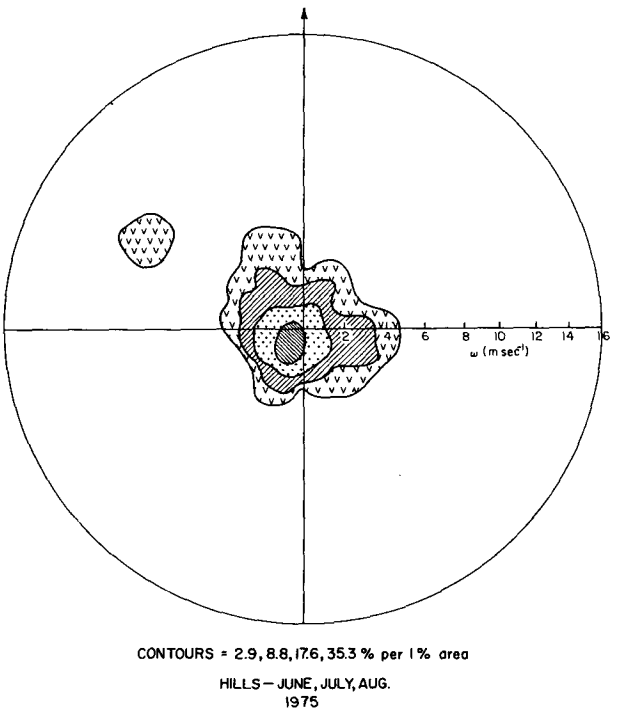

FIG. 2. Fig. 1 point-plot contoured with 1% area circle.

the center of the net to the edge) is equated to 36 mi h^{-1} or 16.1 m s^{-1}.

This diagram is, in effect, a wind velocity probability distribution diagram with data given in percent of the total observations per 1% net area. The actual probability for a given area or sector of the diagram is given by the fraction of total poles in 1% of the area times the percent of the net area comprising the test sector desired. If N_s and N_t are the number of observations within a sector of the projection and the total number of observations, respectively, the mean probability within the sector is found to be

$$\bar{p}_s = \frac{N_s}{N_t} = \left(\frac{\bar{C}_s}{100}\right)\left(\frac{100A_s}{\pi R^2}\right) = \frac{\bar{C}_s A_s}{100\pi}, \qquad (1)$$

where $\bar{C}_s$ is the mean point concentration within the sector in percent per 1% net area, A_s is the area of the sector in square centimeters and R is the radius in centimeters of the Lambert net. In most applications the 10 cm radius net is used.

If it is desired, for example, to obtain the frequency expected for winds coming from the 330–350° compass direction, falling in the velocity range 2.5–5.5 m s^{-1}, we can simply construct this sector over the contoured fabric diagram as shown in Fig. 3 and obtain the necessary information for the calculation. For this case (described by the larger stippled sector of Fig. 3) Eq. (1) gives $\bar{p}_s = 0.030$, and for the high concentration sector in the southwest quadrant of Fig. 3, $\bar{p}_s = 0.051$. In the first case the concentration values were assumed to be the average of the contoured values intersected by the sector boundaries ω_1 and ω_2. In the second case the *maximum* concentration within

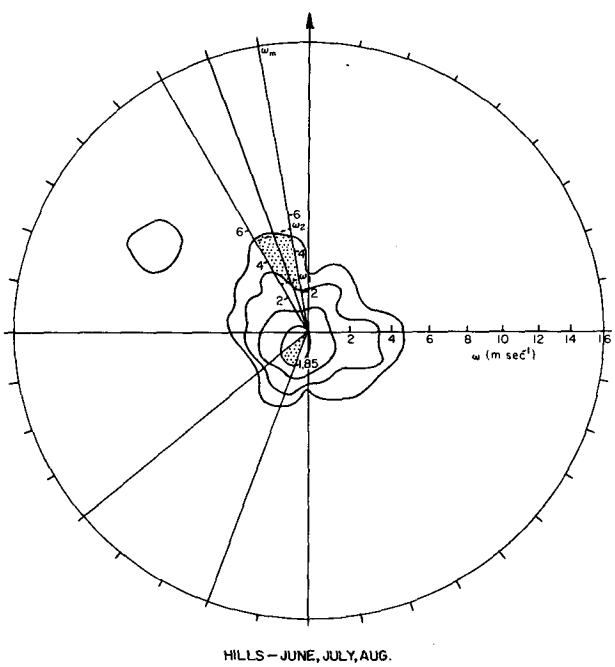

FIG. 3. Sector tests for two regions of the fabric diagram of Fig. 2.

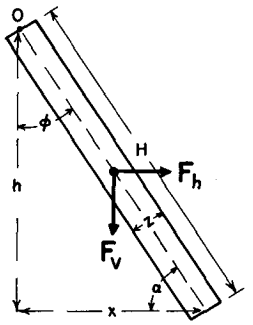

FIG. 4. End view of plat plate fixed at O and suspended at vertical angle ϕ by wind moving from left to right.

the zone was averaged with the outer contour value. To demonstrate that the probability obtained is a reasonably accurate estimate we return to the point plot and note that for a total of 34 poles a probability of 0.030 gives 1.0 points within the large stippled segment and 1.7 within the small stippled segment. This compares to 2 points actually counted within each sector by overlaying the outline of the sectors on the point plot. The calculated probabilities for the entire central and stippled zones of Fig. 2 are 0.126 and 0.303, respectively. This equates to 4.3 and 10.3 points as calculated, compared with 5 and 11 observed. Obviously, better agreement of calculated and observed values will occur with a larger sample or larger test sector.

3. Generalization of the velocity variable

Although plots such as given in Fig. 1 are a practical and valid way to present the data, it is not general in the sense that work from differing areas can be compared. This is likely to be so because of the differing upper limit of the velocity expected from locality to locality and therefore the differing scales that might be required. To generalize the technique and make it applicable for all measurements we have considered the following simple physical model.

In Fig. 4 is shown an end view of a flat square plate hinged at O. A wind vane (not shown) is employed to keep the plate normal to the plane of the maximum wind vector. Under calm winds the plate will hang vertically, making an angle $\phi=0$ with the vertical. Under very strong winds the angle ϕ will increase and, assuming laminar flow and frictionless conditions, the plate will hang at an angle ϕ approaching $\pi/2$. We thus find for plate of mass M and volume H^2Z that equilibrium requires

$$F_v x - F_h h = 0,$$

or

$$\tfrac{1}{2}MgH\cos\alpha - \tfrac{1}{2}F_h H\sin\alpha = 0, \qquad (2)$$

where F_h is the horizontal force required to balance the gravitational force $F_v=Mg$, where g is gravitational acceleration. Now if the plate is to be supported at angle ϕ on its hinge by the force of the wind, then

$$\frac{1}{2}\frac{m\omega^2}{V} = \frac{1}{2}\rho_\alpha\omega^2 = \frac{F_h}{H^2\sin\alpha}, \qquad (3)$$

where m is the mass of air per volume V moving through area $H^2\cos\phi$, $\rho_\alpha=m/V$ is the density of the air and ω the wind velocity. Since from Eq. (2)

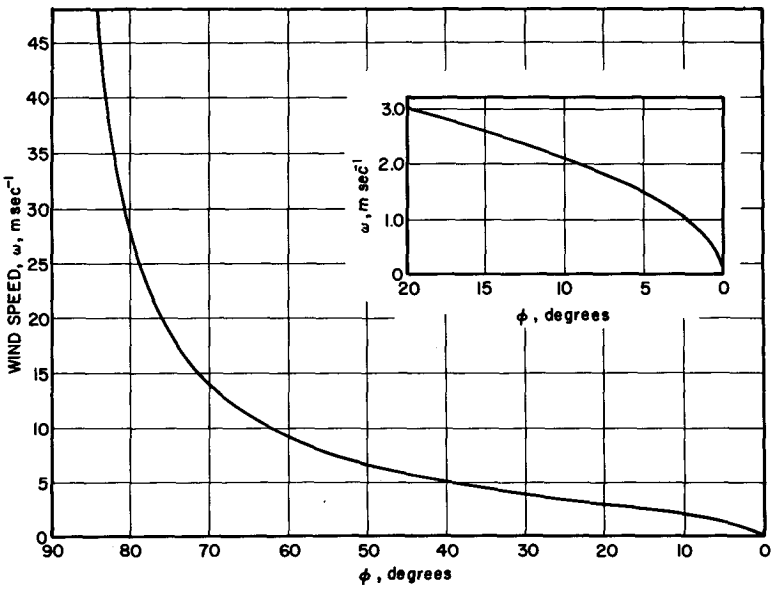

FIG. 5. Wind velocity ω as a function of ϕ for $M=1.35\times10^3$ g, $H=1$ m, $Z=0.05$ cm, $\rho_\alpha=1.11\times10^{-3}$ g cm^{-3}.

$$F_h=\frac{Mg\cos\alpha}{\sin\alpha}=\frac{Mg\sin\phi}{\cos\phi}, \quad (4)$$

we obtain

$$\omega=\left(\frac{2Mg\sin\phi}{\rho_\alpha H^2\cos^2\phi}\right)^{\frac{1}{2}}, \quad (5)$$

or

$$\sin\phi=\sqrt{\xi^2+1}-\xi, \quad (6)$$

where $\xi=Mg/(\rho_\alpha H^2\omega^2)$.

This allows all observations to be plotted on a uniform scale given by (6). Thus, at the center of net we have calm winds ($\phi=0$, $\omega=0$), whereas at $\phi=90°$ wind velocity must be infinite. The actual shape of the function depends somewhat on the plate dimension and mass. It can be shown, however, that in terms of energy or power it is quite arbitrary what value of M and plate dimensions are used and only for convenience in observing the fabric distribution is there a need to select these values carefully. In our analysis we choose the plate to have dimension 1 m^2 and 0.5 mm thick, composed of aluminum (with density of 2.70 g cm^{-3}). Thus, if we let the atmospheric density ρ_α at 900 mb be 1.11×10^{-3} g cm^{-3}, the term $Mg/\rho_\alpha H^2=1.193\times10^5$ cm^2 s^{-2}. For convenience of plotting, ω is shown as a function of ϕ in Fig. 5 for these stipulated conditions.

4. Wind energy analysis

The kinetic energy contained within the wind can be visualized by regarding a unit volume of space through which the air moves. Thus, an increment of *energy density* (in ergs per cubic centimeter, or similar units) can be obtained as the product of the kinetic energy $E(\phi)$ carried by winds for a given value of velocity (or ϕ) and the probability of the winds having that value of velocity for the given locality. Thus, in terms of ϕ we have

$$dE=E(\phi)p(\phi)d\phi, \quad (7)$$

or, introducing the mean value of $E(\phi)$ for a larger sector,

$$E_s=\frac{\rho_\alpha}{2(\phi_2-\phi_1)}\int_{\phi_1}^{\phi_2}\omega_s^2(\phi)p_s(\phi)d\phi \approx\frac{\rho_\alpha\bar{p}_s}{2(\phi_2-\phi_1)}\int_{\phi_1}^{\phi_2}\omega_s^2(\phi)d\phi, \quad (8)$$

where the approximate relationship holds for sectors of the fabric diagram for which the probability gradient is small. Therefore, under the approximate conditions stated, Eq. (8) can be combined with Eqs. (1) and (5) to obtain

$$E_s=\frac{MgA_s\bar{C}_s}{100\pi H^2(\phi_2-\phi_1)}\int_{\phi_1}^{\phi_2}\frac{\sin\phi}{\cos^2\phi}d\phi \quad (9)$$

which reduces to

$$E_s=\frac{0.4211}{(\phi_2-\phi_1)}A_s\bar{C}_s(\sec\phi_2-\sec\phi_1) \quad (10)$$

for the case described above (Fig. 5). One should note that a *sector* is defined on the wind fabric diagram only, and for computational purposes consists of an area A_s (measured in square centimeters) bounded by two compass headings (θ_1,θ_2) and two velocity values $[\omega(\phi_1), \omega(\phi_2)]$. E_s for this sector represents the most probable energy density at the locality for which the data apply, for wind conditions defining the sector boundaries.

Now the *total* energy density of the wind expected at a specific locality is obtained as an integral over all increments of velocity $\omega(\phi)$ as well as over all increments of compass direction θ:

$$E_T=\frac{1}{(\phi_2-\phi_1)}\int_{\phi_1}^{\phi_2}E_s(\theta)d\theta=\frac{\rho_\alpha}{2(\phi_2-\phi_1)}\int_{\theta_1}^{\theta_2}\int_{\phi_1}^{\phi_2}\omega_s^2(\phi)\times p_s(\theta,\phi)d\phi d\theta, \quad (11)$$

where now the probability function itself contains the variables θ and ϕ. It would be extremely unlikely that any function could be obtained from the fabric diagram that would allow direct integration of Eq. (11). However, from a practical standpoint, an array of sectors s throughout the fabric diagram can be plotted on an overlay and specific incremental energy values given by expressions similar to (10) summed according to

$$E_T\approx\frac{Mg}{2\pi H^2}\sum_{\theta=0}^{2\pi}\sum_{\phi=0}^{\pi/2}\bar{C}_s\left(\frac{a+a^{-1}-2}{\phi_2-\phi_1}\right)_s\Delta\theta_R, \quad (12)$$

where $a=\cos\phi_1/\cos\phi_2$.

The relation $(a+a^{-1}-2)\Delta\theta_R$ follows from the product $A_s(\sec\phi_2-\sec\phi_1)$ of (10) with the definition of sector area A_s being

$$\begin{aligned}A_s&=\int\Delta\theta_R dR\\&=2R^2\Delta\theta_R\int_{\phi_1}^{\phi_2}\sin(\phi/2)\cos(\phi/2)d\phi\\&=50\Delta\theta_R(\cos\phi_1-\cos\phi_2),\end{aligned} \quad (13)$$

where R is the diagram (net) radius (cm) and $\Delta\theta_R$ is the sector width (rad).

5. Specific power potential

The power, or work per unit time, can also be determined from the fabric analysis. Referring again to Fig. 4, the volume of air moving against the plate has flux cross section $A_f=H^2\cos\phi$. Thus, the power P

from the wind required to maintain the plate tilted at the angle ϕ against gravity is

$$\text{Power}=\left(\begin{matrix}\text{Volume of air per unit time}\\ \text{moving through area } A_f\end{matrix}\right)\times(\text{Kinetic energy per unit volume})=\text{energy/time}.$$

Mathematically,

$$\begin{aligned}P&=\dot{V}E\\&=(\omega A_f)\left(\frac{m\omega^2}{2V}\right)\\&=\frac{A_f}{2}\rho_\alpha\omega^3,\end{aligned}\tag{14}$$

which, according to Eq. (5), becomes

$$P=\frac{(2Mg\sin\phi)^{\frac{3}{2}}}{2\rho_\alpha^{\frac{1}{2}}H\cos^2\phi}.\tag{15}$$

The power required for a given application depends upon the effective working surface of the device transmitting the wind energy to mechanical or electrical energy. We are thus more interested in *specific power* $\tilde{P}$, or power per unit area. The *potential* for application at a given locality depends on the probability that the winds will have a certain velocity. Hence, based on concepts already treated above, we define $\tilde{P}'$ the *specific power potential* as

$$\tilde{P}'=\tilde{P}p=\frac{Pp}{A_f}.\tag{16}$$

For a given finite sector (s) of the wind fabric diagram, we use (9) to write

$$\tilde{P}_s'=\frac{\rho_\alpha}{2(\phi_2-\phi_1)}\int_{\phi_1}^{\phi_2}\omega_s^3(\phi)p_s(\phi)d\phi\approx\frac{\rho_\alpha\bar{p}_s}{2(\phi_2-\phi_1)}\int_{\phi_1}^{\phi_2}\left(\frac{2Mg\sin\phi}{\rho_\alpha H^2\cos^2\phi}\right)^{\frac{3}{2}}d\phi\tag{17}$$

$$=\frac{(2Mg)^{\frac{3}{2}}\bar{p}_s}{4H^3\rho_\alpha^{\frac{1}{2}}(\phi_2-\phi_1)}\left[\frac{(\sin\phi_2)^{\frac{3}{2}}}{\cos^2\phi_2}-\frac{(\sin\phi_1)^{\frac{3}{2}}}{\cos^2\phi_1}\right].\tag{18}$$

A summation over ϕ and θ can be accomplished for an array of finite sectors of the fabric diagram, similar to the method described for energy [Eq. (12)]:

$$\tilde{P}_T'=\frac{1}{2\pi}\sum_{\theta=0}^{2\pi}\sum_{\phi=0}^{\pi/2}\bar{C}_s\left[\frac{f(\phi_2)-f(\phi_1)}{(\phi_2-\phi_1)}\right]_s\times(\cos\phi_1-\cos\phi_2)_s\Delta\theta_R,\tag{19}$$

where

$$f(\phi)=\frac{(2Mg)^{\frac{3}{2}}}{4H^3\rho_\alpha^{\frac{1}{2}}}\left[\frac{(\sin\phi)^{\frac{3}{2}}}{\cos^2\phi}\right].$$

A log plot of $f(\phi)$ is presented in Fig. 6.

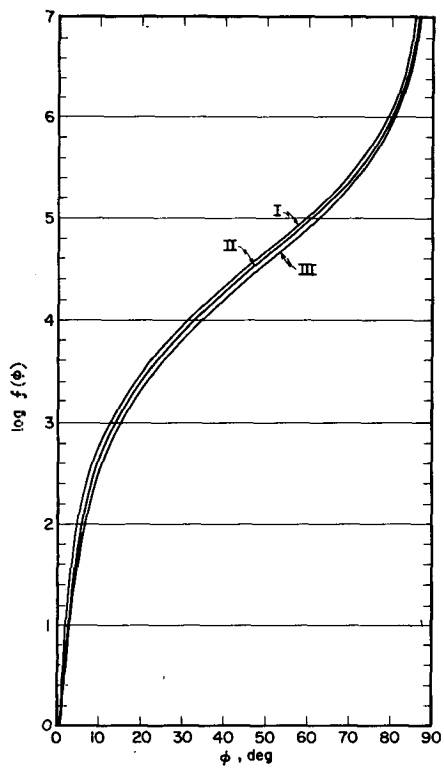

FIG. 6. The quantity $\log f(\phi)$ as a function of ϕ for swinging plate of $H=1$ m, $Z=0.05$ cm, $M=1.35\times10^3$ g, in air of density $\rho_a=1.11\times10^{-3}$ g cm^{-3}.

It should be remembered that although the expressions leading to E_s and $\tilde{P}_s'$ were derived on the basis of the "swinging plate" model, the results obtained from actual wind vector data are of general application and not dependent upon the model used. We have simply employed this "artifice" to plot wind vector data on the Lambert projection; these data are incorporated into the expressions leading to wind energy and power which are dependent only upon the data sample used to prepare the wind fabric diagram.

The actual wind energy and the velocities required to suspend the plate at angle ϕ is dependent on air density which, of course, is a function of composition, temperature and station pressure. Thus we can increase the versatility of the technique and accuracy of the calculations by assuming ρ_α to have the function (WMO Paper 188):

$$\rho_\alpha=3.484\times10^{-4}P/T_v',\tag{20}$$

where P is the atmospheric pressure (mb) and T_v' the adjusted virtual temperature (K). This relation re-

TABLE 1. Selected values of ϕ (deg) for typical and extreme values of ρ_α.

Case	ρ_α (g cm^{-3})	Wind velocity ω (m s^{-1}) 0.5	2.5	15.0	30.0
I*	0.77×10^{-3}	0.4	10.1	67.9	78.8
II**	1.11×10^{-3}	0.6	14.3	71.5	80.7
III†	1.32×10^{-3}	0.8	18.1	73.8	81.9

* $T_v'=318$ K, $P=700$ mb, $\gamma=0.053$.
** ICAO atmosphere at 1000 m, $T=282$ K, $P=898.7$ mb.
† $T_v'=T=263$ K, $P=1100$ mb, $\gamma=0$.

duces ξ of (6) to

$$\xi=\frac{3.797\times10^5 T_v}{\omega^2 P} \tag{21}$$

$$=\frac{3.797\times10^5 T(1+0.61\gamma)}{\omega^2 P}, \tag{22}$$

where T is the ambient air temperature (K) and γ the water vapor mixing ratio (g g^{-1}). The value of ϕ, and hence the point positions, are only slightly affected by even large extremes in air density. Table 1 presents these extremes as cases I and III in comparison to a typical value, case II, of moderate station pressure and temperature. The data for case II were used for preparation on Fig. 5 and all Black Hills wind fabric diagrams presented here. The slight density changes expected for weather variations in the Black Hills will not change the fabric pattern appearance significantly. However, there is a 71.4% difference in the extremes in ρ_α shown by cases I and III; both energy and power will differ by this same amount—a fact which may be significant in actual applications.

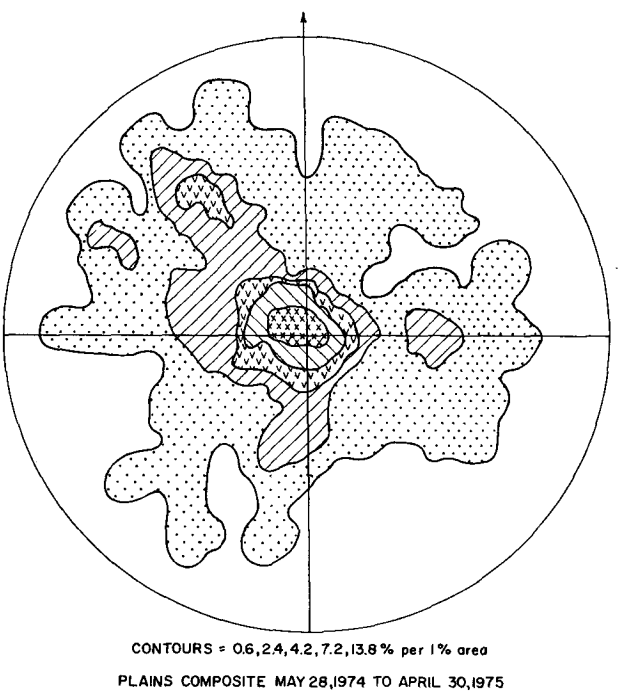

FIG. 7. Wind fabric diagram for 167 vectors over plains of western South Dakota, 1974–75.

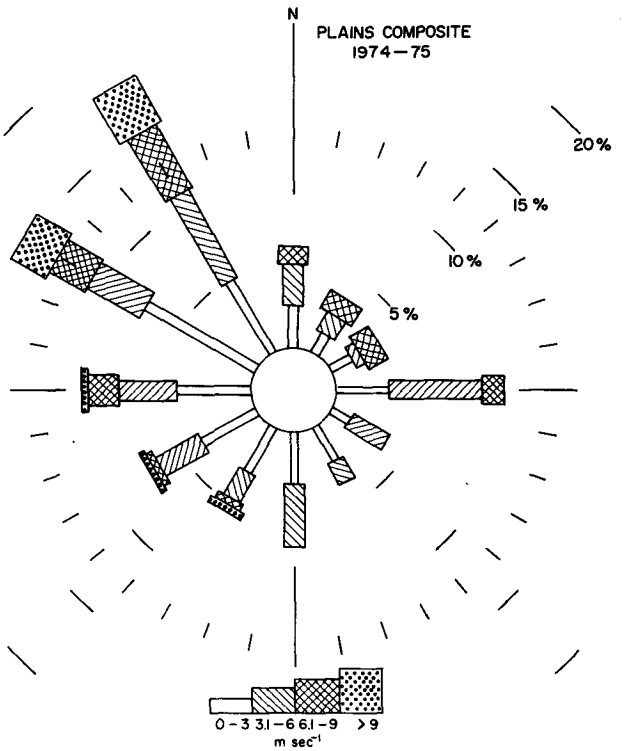

FIG. 8. Rose diagram for 167 wind vectors of Fig. 7.

6. Application to a specific data sample

As an illustration of the technique, wind vector data for a portion of western South Dakota for the years 1974 and 1975 (beginning mid-May) are presented in a fabric diagram (Fig. 7) and a rose diagram (Fig. 8). This fabric combines data from seven stations on the prairies surrounding the Black Hills and contains 167 measurements. Our analysis will therefore represent average conditions over the prairies of western South Dakota in the vicinity of the Black Hills. At first appearance one might be tempted to find a function which would approximate the p distribution which appears to be axial symmetric and roughly bell-shaped. No function could be determined, however, which would allow ready evaluation of the double integral of Eq. (11).

As an example of the calculation of the energy density for one sector we select a portion of the dia-

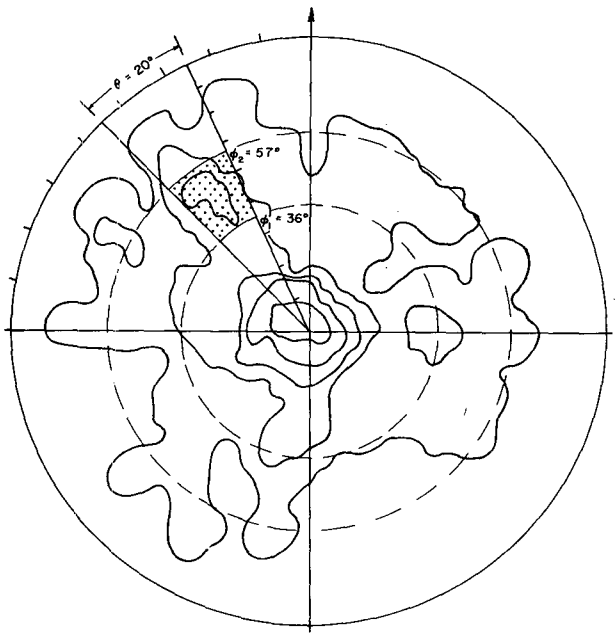

FIG. 9. Sector analysis of high velocity anomaly between $\phi=36$ and 57°, and $\theta=315$ and 335°.

gram, indicated in Fig. 9, that lies within the compass interval 315–335° and contains $\phi_1=36°$ and $\phi_2=57°$. The average contour value within this sector was found to be 3.9% per 1% area. Thus, we find from Eq. (1) that $\bar{p}_s=0.057$, and from Eq. (10), $E_s=12.4$ ergs cm^{-3}. Using Eq. (18), we find

$$\tilde{P}'_s=8.9\times10^3 \text{ erg cm}^{-2}\text{ s}^{-1}.$$

From examination of the fabric distribution of Fig. 6 it would seem that this sector should contain the highest power potential within the entire wind velocity distribution. As can be seen, a positive fabric anomaly exists in that position and a breakdown of the data into calendar quarters shows that the higher frequencies here come from the winter and early spring months.

The fabric of Fig. 7 was then broken down into 10° $\Delta\phi$ and $\Delta\theta$ sectors,[2] and $\bar{C}_s$ was determined for each sector as the mean of the two contours enclosing the fabric area containing the sector (e.g., 5.85% per 1% area for the large sector of Fig. 3) except that $\bar{C}_s$ was set at zero for areas outside the first contour. Values for sectors containing a contour line were obtained simply by proportion of the areas within the sector. Calculations according to (12) and (19) were made for the resulting 324 sectors of the fabric diagram. The resulting E_s and $\tilde{P}'_s$ values for the four compass quarters are as follows:

	NE	NW	SW	SE	Total
ΣE_s (erg cm^{-3})	34.04	134.41	61.25	23.39	253.09
$10^{-4}\Sigma P'_s$ (erg cm^{-2} s^{-1})	2.92	16.98	7.21	1.63	28.74

It is now seen that the specific power potential calculated for the abovementioned anomaly lying between $\phi_1=36°$ and $\phi_2=57°$ is only about 1/17 of that obtained for the entire northwest quadrant for the data sample given. A breakdown of the northwest quadrant data reveals that a much greater contribution to both E_s and $\tilde{P}'$ comes from the $\Delta\phi=70$–80° sectors even though in many sectors $\bar{C}_s$ is zero with the maximum value being 1.1. Thus, a few high-velocity wind measurements greatly influence the total energy and power potential. This suggests that ϕ_{max} for such diagrams be restricted to the furling point or some practical limit imposed by the wind generating system to be used for the area under consideration.

As expected for the Black Hills 1974–75 data, the greatest energy comes from the northwest quadrant, followed by the southwest and northeast quadrants; note the much lower value from the southeast quadrant. In normal years, a higher energy density would be expected from the southeast quadrant, but for the period studied only a very few southeast wind observations were noted.

These calculations have served to demonstrate the remarkable influence of velocity and probability on wind energy density. For example, for the northwest quadrant of the Black Hills data just discussed the 10–20° segment in ϕ and a vector point density $\bar{C}_s$ of 9.3% per 1% area gives an energy density of only about 1/70 of that observed in the 70–80° segment having a point density of only 0.5% per 1% area!

It should be recalled that the example given here pertains to average conditions over western South Dakota.[3] More likely, however, such an analysis would be performed using a large data base at one locality, giving results which would more profitably be used in wind energy applications. The total energy and power quantities obtained from the double summation processes of Eqs. (12) and (19) are thus the values expected for all directions and velocities of wind experienced at a given locality. The values expected at any locality will be a function of the time of day, or season; this would suggest that fabric diagrams be prepared for any diurnally or seasonally stratified sample needed for a specific application. Once the data are plotted, the specific power or specific power

[2] This grid density appears about optimum. Unless several wind velocity observations exist between $\phi=80$ and 90° ($\omega>28$ m s^{-1}), smaller sectors add very little to the accuracy of the calculations.

[3] The 28.74 erg cm^{-2} s^{-1} (287 W m^{-2}) obtained is in reasonable agreement with the annual average wind power map of Ramakumar *et al.* (1974) where western South Dakota falls in the zone between 200 and 250 W m^{-2}.

potential can be calculated for any fabric sector desired and applied to a given wind energy system.

Acknowledgments. This work was sponsored by the State of South Dakota. Mr. Donald Blair assisted in preparation of the fabric diagrams.

APPENDIX

The Stereographic and Equal-Area Projections

1. Construction of the projections[4]

The stereographic projection has long been used in crystallography, structural petrology, structural geology and civil engineering for solutions to many geometric problems. The great advantage in the Wulff stereographic projection and its peripherally distorted counterpart, the Lambert equal area projection, lies in the ability for the user to "view" the positions of planes and lines in space.

Fig. 10A illustrates a sphere with center at O and containing an equatorial circle (EC) which defines the *equatorial plane.* Any point lying on the surface of this "reference" sphere, such as point P, can be transferred to the equatorial plane by projecting the point through the sphere and equatorial plane to the lower pole O′. The general formula for locating the projected point P′ on the stereographic equatorial plane of reference sphere of radius R is

$$r = \mathrm{OP}' = R \tan\left(\frac{\phi}{2}\right), \qquad \text{(A1)}$$

where ϕ is the zenith angle of the line OP. The line OP generally represents an intersection of two planes or the normal to a plane oriented in space. This line may represent lineations in metamorphic surfaces or normals to joints or other planar petrologic elements in geology, and hence is a vector quantity (with each lineation or joint being of unit magnitude).

The sphere may be regarded as having parallels and meridians. The projection of the parallels and meridians onto the equatorial plane by means of Eq. (A1) results in the stereographic projection (Fig. 10B). It should also be noted that the traces of planes can also be plotted on the stereographic projection, although it is generally more convenient to plot the plane normal as a pole. The following definitions are helpful:

1) A *great circle* is the trace of the intersection of any plane with the reference sphere when the plane passes through the center of the sphere. It is the largest circle that can be described on the sphere. The equator and all meridians are great circles.

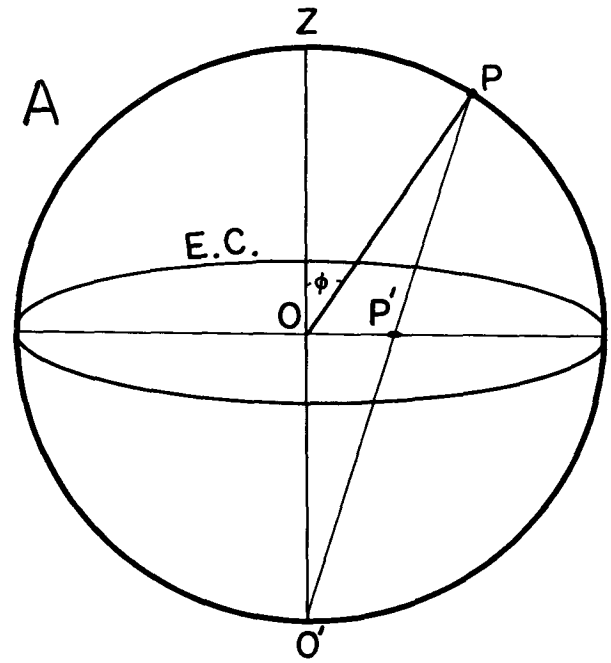

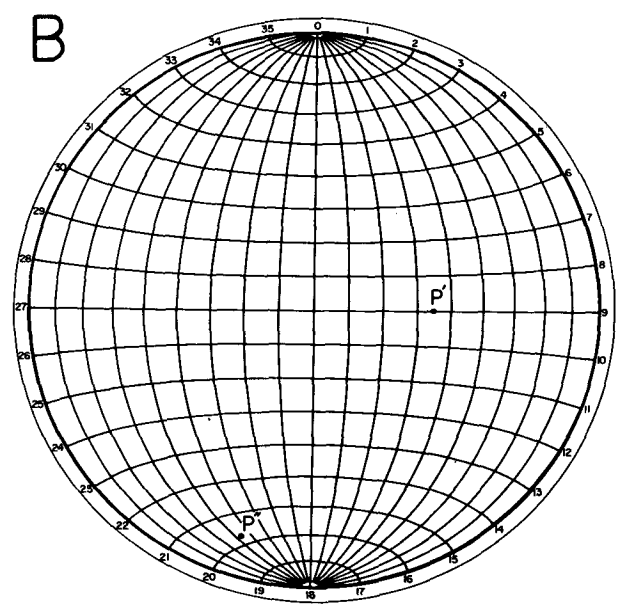

FIG. 10A. Reference sphere with pole OP having zenith angle ϕ and compass direction 90°. Point P′ on the equatorial plane (defined by circle EC) is obtained by projection of P through equatorial plane to O′.

FIG. 10B. Lambert equal area projection with meridians and parallels at 10° intervals. P′ and P″ are also plotted (see text).

2) A *small circle* is the trace of the intersection of any plane passing through the reference sphere but not through its center. All parallels of latitude except the equator are small circles.

[4] This discussion of stereographic (Wulff) and equal-area (Lambert) projections makes use of material from Higgs and Tunell (1959), Fairbairn (1949) and Turner and Weiss (1963).

3) The *upper* and *lower hemispheres* are the spherical halves containing radii OZ, and OO′, respectively. In all projection work, only one sphere is used. In structural geology, it is generally the lower hemisphere and in crystallography it is generally the upper hemisphere.

In the wind fabric work described herein, the upper hemisphere is used with OP (Fig. 10A) representing the intersection of the suspended aluminum plate and a vertical plane containing the wind direction. In this case, since only one angle is used to describe the wind direction (it being assumed horizontal), the angle ϕ remains undefined and is used to describe the magnitude of the wind velocity by means of the swinging plate artifice described in the text.

The Lambert equal area projection (also known as the Schmidt net) is used in the same manner as the stereographic projection as far as plotting is concerned. The meridians and parallels are distorted, however, to permit the projection of an area element of the reference sphere onto the equatorial plane such that a projected unit area is identical (in magnitude) anywhere on the equatorial section, regardless of its position on the reference sphere. It is emphasized here that one must *not* use the stereographic projection for point contouring. However, problem solving using the angles and relations between points and planes on the Schmidt equal area net may be accomplished in the usual manner (see Turner and Weiss, 1963, pp. 52–58).

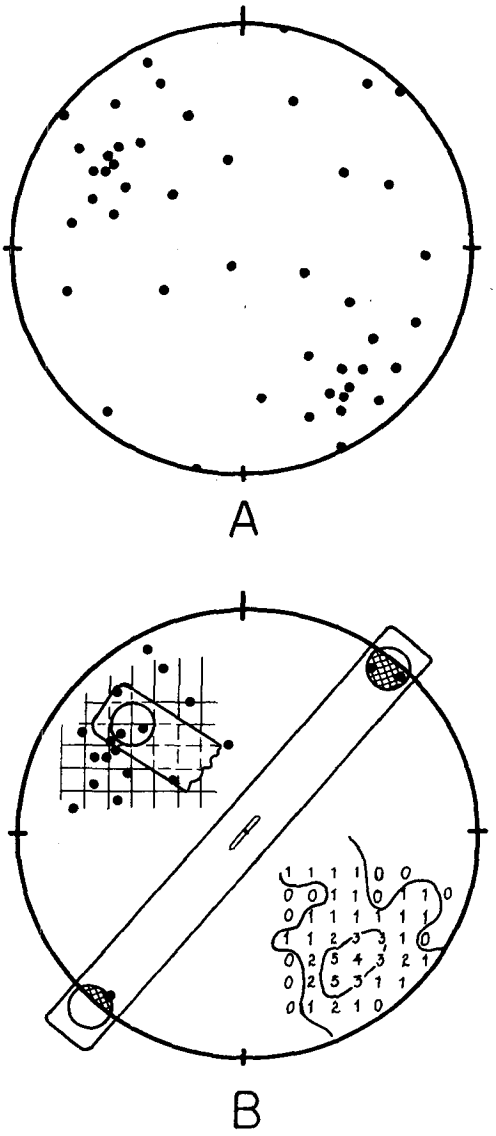

FIG. 11A. Plot of 45 poles on Lambert net overlay. North or zero compass direction located at top of circle.

FIG. 11B. Poles of northwest quadrant of Fig. 11A superimposed over centimeter grid. A portion of the 1% area counter is shown. The number 2 is to be plotted at the center of the circle where the grid lines intersect. The poles of the southeast quadrant of Fig. 11A have been counted and contoured as shown. The method of counting at the net edge using the double-hole counter is also illustrated.

2. Method of plotting of data

The Lambert projection is best mounted on a heavy piece of cardboard with a thumbtack protruding upward from the center (O) of the projection.[5] A piece of tracing paper is placed over the projection onto the thumbtack and the north or zero point marked. If, in Fig. 10A, ϕ is 35°, the point is plotted on the Lambert equal area projection as in Fig. 10B. To be more general, we assume a pole oriented in space with zenith angle ϕ of 75° and a compass direction of 197°. With the north position marked on the overlay, the overlay is rotated so that the 197° compass direction falls along any east-west or north-south diameter of the net. The ϕ angle (75°) is marked along the diameter from the center O toward the edge of the projection. The point is then plotted and the overlay returned to its initial (reference) orientation. The point P″ in Fig. 10B represents the position of this pole.

In actual fabric construction, a large number of points will be plotted in this manner and Fig. 11A represents a hypothetical data set of 45 such points. One now may contour the plotted data to provide a basis for statistical analysis of the concentration distribution. A piece of centimeter paper is placed underneath the overlay with an exact 20 cm distance adjusted to coincide with the two diameters of the projection.

[5] 20 cm Lambert (Schmidt) projections may be obtained from the Department of Geology, Johns Hopkins University, Baltimore, Md. 21218, at a cost of 50¢ each. For this net $r = 2^{\frac{1}{2}}R \sin(\phi/2)$.

Next it is necessary to sum the points within 1% of the net area by means of a special template illustrated in Fig. 11B. This template is made simply by boring a 2 cm diameter hole in a 3–5 mm thick strip of transparent plastic. The most convenient type of template is one containing two holes, the centers of which are positioned exactly 20 cm apart such that points near the edge of the projection can be counted in a 1% area by using both circles as illustrated in Fig. 11B. The number of points falling within the 1% area circle is then written in at the intersection at the centimeter grid at the center of the circle. This is continued at either 1 or $\frac{1}{2}$ cm intersection intervals throughout the entire projection.

The contouring is accomplished by smoothly connecting lines of equal numbers as illustrated in the lower right-hand quadrant of Fig. 11B. The contours are then labeled as percent poles per 1% net area. If the total number of poles for the example given in Fig. 11 is 45, then the contour representing three poles per 1% area is found to be 6.67% per 1% net area. Generally a contour separating the O region from the rest of the data is included and only sufficient additional contours added to clearly portray the fabric features.

3. Statistical tests for fabric homogeneity

There have been many requirements in structural geology and crystallography for statistical methods to test for fabric homogeneity or to determine whether certain fabric features are real or apparent. This same requirement may arise in wind fabric analysis. A detailed description of such tests is beyond the scope of this presentation, but the methods are very similar to those used in meteorological statistics and involve the breakup of the fabric pattern into zones or samples which may be studied by means of chi-square tests or similar procedures. [For further information, the reader is referred to Chap. 23 of Fairbairn (1949) or the references in Turner and Weiss (1963, p. 64).]

REFERENCES

Fairbairn, H. W., 1949: *Structural Petrology of Deformed Rocks.* Addison-Wesley, 344 pp.

Higgs, D. V., and G. Tunell, 1959: *Angular Relations of Lines and Planes.* W. C. Brown Co., 42 pp.

Letestu, S., Ed., 1966: International Meteorological Tables (with 1973 amendments). WMO No. 188, TP94.

Ramakumar, R., H. J. Allison and W. L. Hughes, 1974: Wind power—significant? *Proc. Second Western Energy Conf.*, South Dakota School of Mines and Technology, Rapid City, 3-0 to 3-27.

Turner, F. J., and L. E. Weiss, 1963: *Structural Analysis of Metamorphic Tectonites.* McGraw-Hill, 545 pp.